OCEANOGRAPHY

Chasing iron bioavailability in the Southern Ocean: Insights from *Phaeocystis antarctica* and iron speciation

Marion Fourquez[1,2]*, David J. Janssen[3], Tim M. Conway[4], Damien Cabanes[2], Michael J. Ellwood[5,6], Matthias Sieber[4,7], Scarlett Trimborn[8], Christel Hassler[2,9,10]

Dissolved iron (dFe) availability limits the uptake of atmospheric CO_2 by the Southern Ocean (SO) biological pump. Hence, any change in bioavailable dFe in this region can directly influence climate. On the basis of Fe uptake experiments with *Phaeocystis antarctica*, we show that the range of dFe bioavailability in natural samples is wider (<1 to ~200% compared to free inorganic Fe′) than previously thought, with higher bioavailability found near glacial sources. The degree of bioavailability varied regardless of in situ dFe concentration and depth, challenging the consensus that sole dFe concentrations can be used to predict Fe uptake in modeling studies. Further, our data suggest a disproportionately major role of biologically mediated ligands and encourage revisiting the role of humic substances in influencing marine Fe biogeochemical cycling in the SO. Last, we describe a linkage between in situ dFe bioavailability and isotopic signatures that, we anticipate, will stimulate future research.

INTRODUCTION

Our understanding of the link between iron (Fe) utilization by phytoplankton in surface waters and carbon storage in the deep ocean has evolved from the Fe hypothesis (*1*) over 30 years of investigations. This motivation to better understand the role of the micronutrient Fe in global biogeochemical cycles has led to an explosion of research, including rapid modeling developments (*2*–*4*) and enhanced global sampling initiatives at the international level such as GEOTRACES (*5*). These efforts have resulted in large scale maps of the distribution of dissolved Fe (dFe; operationally defined as size range < 0.2 μm), the discovery of a multitude of oceanic Fe sources, and better understanding of the processes that control the marine Fe cycle (*6*). However, in environments such as the surface Southern Ocean (SO), where Fe is the limiting factor for large-scale ecosystem processes and carbon dioxide (CO_2) drawdown (*7*, *8*), the capacity of the phytoplankton community to take up dFe—rather than the absolute concentrations of dFe in surface waters—is what ultimately matters to understand surface productivity.

To date, describing the bioavailability of dFe in the surface SO relies on the accuracy of chemical methods that quantify dFe at vanishingly low concentrations [e.g., 10 to 50 pM; (*9*)]. Although the international GEOTRACES program has made tremendous strides in mapping the distribution (*10*, *11*) and speciation (*12*–*14*) of dFe, the concept of "bioavailability" itself remains uncertain because the correlation between in situ dFe concentration and biological uptake is not straightforward. This uncertainty stems from the fact that only a small fraction of the dFe, defined as the free inorganic Fe (Fe′), is thought available to be directly taken up by microorganisms to support their metabolism and growth (*15*–*17*). In fact, dFe is mostly bound to natural organic ligands (FeL) in seawater (*18*, *19*). In SO waters, the concentration of Fe′ is generally insufficient to satisfy biological demand (*20*), so that phytoplankton must acquire Fe from the ligand bound pool (>95% of dFe) to satisfy their growth requirements (*21*–*25*). Biological Fe uptake thus depends not only on dFe and Fe′ concentrations in the immediate surroundings of the cells (*15*) but also on the chemical nature and the strength of the Fe-binding organic ligands (*16*, *21*, *25*, *26*). Diverse groups of organic ligands are regarded as critical players in Fe speciation (*12*, *13*, *27*, *28*), but the exact role of many of these complexes remains unclear. For instance, few studies have stressed the role of electroactive humic substances (eHS) (*29*, *30*) or products of phytoplankton degradation (*31*) on Fe speciation. Further, the potential contribution of different compounds to the complexing pool of ligands is mostly unresolved for most of the SO and for the oceans as a whole.

For microorganisms, a combination of biological (membrane transport), chemical (metal-ligand dissociation kinetics), and physical (diffusion) reactions are at play to overcome Fe limitation (*16*, *32*), resulting in many confounding effects in field studies. Strategies of Fe uptake in states of Fe deficiency are well documented for phytoplankton [e.g., (*33*–*35*)], but large variations of observed in situ Fe uptake measurements cannot be fully explained by variations in dFe concentrations. Despite this, dFe bioavailability in the ocean is often either described by reference to in situ dFe levels or Fe uptake measurements. In addition, it remains difficult to draw comparisons between studies as different microbial assemblages—in terms of diversity, abundance, and physiology—are investigated. To overcome this issue, recent studies have instead aimed to assess dFe bioavailability using the ratio of Fe uptake rate to phytoplankton cell surface area (S.A.) and dFe concentrations (*3*, *36*, *37*). This approach involves conducting Fe uptake bioassays to determine the

[1]Aix Marseille Univ., Université de Toulon, CNRS, IRD, MIO UMR 110, Marseille 13288, France. [2]University of Geneva, Department F.-A. Forel for Environmental and Aquatic Sciences, Geneva 1211, Switzerland. [3]Department Surface Waters, Eawag–Swiss Federal Institute of Aquatic Science and Technology, Kastanienbaum, Switzerland. [4]College of Marine Science, University of South Florida, St. Petersburg, FL 33701, USA. [5]Research School of Earth Sciences, Australian National University, Canberra, ACT, Australia. [6]Australian Centre for Excellence in Antarctic Science, Research School of Earth Sciences, Australian National University, Canberra, ACT, Australia. [7]Institute of Geochemistry and Petrology, ETH Zürich, Zürich, Switzerland. [8]Alfred Wegener Institute, Helmholtz Center for Polar and Marine Research, Bremerhaven 27570, Germany. [9]Institute of Earth Sciences, University of Lausanne, Lausanne 1015, Switzerland. [10]School of Architecture, Civil, and Environmental Engineering, Ecole Polytechnique Fédérale de Lausanne, Sion 1951, Switzerland.
*Corresponding author. Email: marion.fourquez@gmail.com

bioavailability of dFe in natural seawater samples drawn from the observation that several Fe-limited eukaryotic phytoplankton taxa acquire Fe′ at identical rates for a given dFe concentration when accounting for their S.A. (*36*, *38*, *39*). Other studies (*40*, *41*) suggest that rates of Fe uptake by phytoplankton are driven by Fe chemistry (i.e., Fe speciation) and that phytoplankton have uptake rates that can be satisfied by Fe′ diffusivity and kinetic supply rate (including FeL dissociation). This would indicate that dFe bioavailability can be predicted on the basis of Fe speciation. These findings were recently extended to modeling (*3*) by introducing the use of Fe uptake rate constants ($k_{in\text{-}app}$) computed by combining data on cellular Fe to carbon ratio (Fe:C), growth rates, and dFe concentration. Under these circumstances, one can assume that similar phytoplankton affinity for Fe exists for SO phytoplankton species and that a single model organism can serve to determine the bioavailability of dFe in natural seawater samples.

Here, we used the model organism *Phaeocystis antarctica*, an ecologically and biogeochemically important species across the SO (*42*–*44*), to evaluate dFe bioavailability in natural seawater samples. Our data complement the limited information available to date in the SO, allowing a critical evaluation of the emerging global consensus on dFe bioavailability and the prominent role of eHS for this specific ocean region. We determined dFe bioavailability in a comparable way across different sites using six high depth resolution profiles from the upper 500 m of the water column. The selected sites for the vertical profiles include three locations near the Balleny islands, two inside the Mertz glacier polynya, and one in the Ross Sea. The high-resolution nature of our shallow subsurface dataset enables us to investigate the influence of Fe speciation and various physicochemical drivers on dFe bioavailability in contrasting sites in the SO.

RESULTS

Contrasting environments are evidenced by variations in dFe concentrations and the nature, binding constants, and concentrations of Fe ligands

In the Pacific sector of the SO, below the Antarctic Circumpolar Current (ACC; Fig. 1), levels of macronutrients, such as nitrates (Fig. 1A), were consistently high across all six sites, and dFe concentrations in the surface did not exceed 0.08 nmol/liter (Fig. 1B and Table 1), typical for the high-nutrient low-chlorophyll area. While chlorophyll a (Chl a) concentration (*45*) was above 1 μg/liter at two sites within the Mertz glacier polynya (TMR11 and TMR12, with 1.9 and 1.6 μg/liter, respectively), it was relatively low at the other sites, ranging from 0.08 μg/liter (TMR13) to 0.58 μg/liter (TMR14), with open ocean sites sitting in the middle with an average value of 0.24 μg/liter (0.09 for TMR15 and 0.39 for TMR16). Nutrients and dFe concentrations and dissolved δ^{56}Fe for the six different stations are reproduced from (*9*, *46*). These measurements are implemented with Fe speciation data and dFe bioassays to evaluate dFe bioavailability.

Across all water column samples, concentrations of dFe and total ligand ($L_T = L_1 + L_2 + L_3$) ranged between 0.02 and 0.59 nmol/liter and 0.41 and 15.7 nmol/liter, respectively, with ligand conditional stability constants ($\log K'_{Fe'L}$) from 10.2 to 12.4 (Table 1). In general, dFe profiles are nutrient type (*9*, *46*), with surface depletions and subsurface enrichments (fig. S1). However, the ferricline was found below the nutricline, indicating that insufficient Fe is supplied by vertical mixing relative to macronutrients for phytoplankton growth in surface waters (*46*). In the euphotic zone (0 to 100 m), dFe concentrations varied between 0.02 nmol/liter (stations TMR15 and TMR16) and 0.33 nmol/liter (station TMR14) and showed a near-linear trend with values reaching 0.27 nmol/liter (station TMR12) to 0.47 nmol/liter (station TMR15) at 500-m depth (Table 1). Three operationally defined ligand classes were identified: L_1 ($\log K'_{Fe'L} > 12$, $n = 2$), L_2 ($11 < \log K'_{Fe'L} < 12$, $n = 22$), and L_3 ($\log K'_{Fe'L} < 11$, $n = 22$), and Fe′ concentrations were calculated as just 0.01 to 6.76 pmol/liter across the dataset. The strongest ligands (L_1) were only measured at stations TMR16 (open ocean) and TMR13 (islands) at 15- and 75-m depth, respectively. Ligands from the weakest class (L_3) were found at all stations but, particularly, at TMR12 (Mertz glacier polynya), where they were found in 9 of the 11 sampled depths. Overall, L_T constantly exceeded dFe concentrations (Table 1). The highest excess ligand concentrations (ligands not bound to Fe) were found at TMR14 just below the ferricline (40 m) with an excess reaching up to 15.7 nmol/liter.

Our study also explored the composition of this bulk ligand pool by looking at the variability of eHS and hydrolysable carbohydrate (referred to as TPZT). During this transect, eHS concentrations were generally high (>10 μg/liter) and ranged between 4.1 and 329 μg/liter, corresponding to Fe-binding ligand contribution of 0.07 to 5.56 nmol/liter L_T [1 to 188% of L_T, considering that eHS behaves as minimum Fe-binding capacities for terrestrial standard Suwannee River fulvic acid (SRFA) and that SRFA (100 μg/liter) can bind 1.69 nmol/liter Fe (*29*, *30*)] (Fig. 2). The average L_T contribution of eHS was 36 ± 40% ($n = 33$). Further, and despite large variability between samples, we found a positive and significant correlation between L_T and eHS [correlation coefficient (r) = 0.425, $P = 0.01$, $n = 33$], further indicating the relative importance of eHS to the Fe-binding ligand pool to these samples. To constrain the contribution of eHS to the Fe-ligand pool as in (*29*), we plotted an envelope that encompasses the maximum [Suwannee River humic acid (SRHA)] and minimum (SRFA) Fe-binding capacity for eHS (as nanomolar per liter Fe equivalent) together with profiles concentrations of dFe and L_T (Fig. 2).

We find that, on average, dFe concentrations regularly fall below the lower limit of the mean Fe-binding capacity of eHS (Fig. 2), with few values falling just within the lower end of the envelope. We calculated the ratio of dFe to eHS (as nanomolar per liter Fe equivalent) following (*29*). At TMR11, we found a strong and significant correlation between dFe/eHS and depth ($r = 0.92$, $P = 0.001$, $n = 7$), suggesting undersaturation of eHS with Fe at depth. Given that the nature of eHS is still unknown (*29*) and that it might vary with depth due to the activity of the microbial pump (*24*, *28*, *47*), implications for these observations are not straightforward. However, as carboxylic groups—largely present in humic substances and in marine dissolved organic matter—can bind other metallic cations, this undersaturation suggests that eHS has the potential to bind several key trace elements and modulate their marine cycle and residence time. No significant correlation between dFe/eHS and depth was found at any other stations, although nearly all data also show undersaturation of eHS with Fe at depth. By contrast, TPZT concentrations decreased with depth across all stations, consistent with these compounds being labile organic carbon likely rapidly transformed with depth as dissolved organic carbon (*48*) or polysaccharides (*21*).

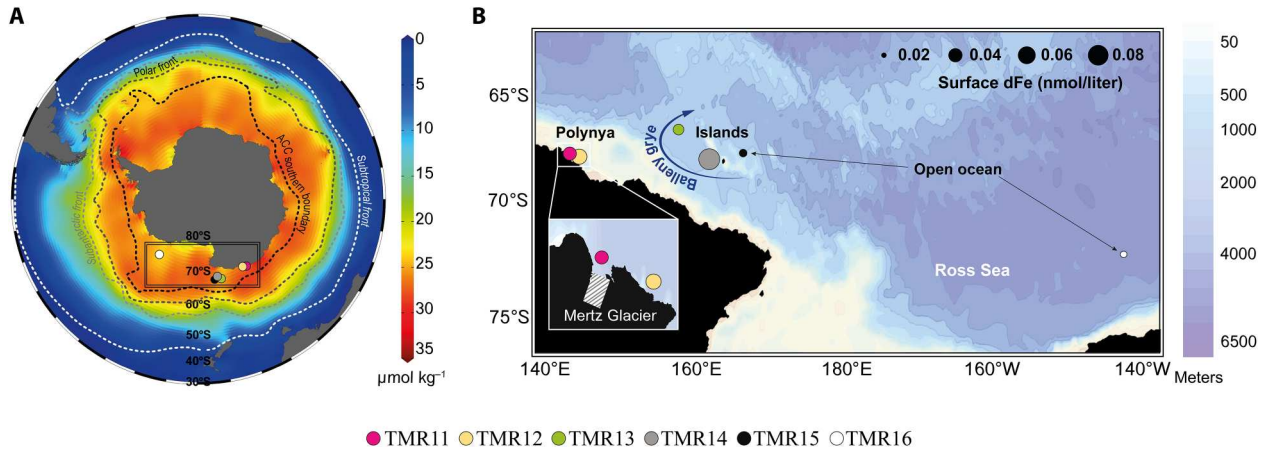

Fig. 1. Station sampling locations from the Antarctic Circumnavigation Expedition (GEOTRACES Compliant Cruise GSc01) leg 2 in austral summer December 2016 to March 2017 for the study. (**A**) Orthographic projection of the SO. Representative positions of the subtropical front, subantarctic front, polar front, and Antarctic Circumpolar Current southern boundary are shown in white, light gray, dark gray, and black dashed lines, respectively. Surface nitrate concentrations are taken from the World Ocean Atlas, 2013 (*59*). (**B**) Close-up map of the sampling area. Stations are identified individually by color and group by sector: Mertz glacier polynya, Balleny islands, and Ross Sea with bathymetry as background. Size of dots is proportional to dFe concentration (nmol/liter) in surface waters.

dFe bioavailability to *P. antarctica* varies widely and is related to proximity to Fe source

We estimated dFe bioavailability based on Fe uptake experiments using the radiotracer ^{55}Fe and the Fe-limited cultures of single-celled *P. antarctica* (see Materials and Methods). More than 200 incubation experiments with ^{55}Fe were conducted to compare rates of Fe uptake by *P. antarctica* in the presence of natural Fe-ligand assemblages for 47 seawater samples. The first result is an unexpectedly wide range of dFe bioavailability that is not related to depth (Fig. 3). Across all samples, the calculated bioavailability ranged from less than 1% to more than 150% of dFe available (relative to Fe′). Note that values greater than 100% indicate Fe uptake at higher rates than expected if dFe were entirely inorganic (i.e., dFe = dFe′), which supports the idea that several Fe uptake mechanisms are used by *P. antarctica* to access dFe (*49*). These enhanced Fe uptake rates have been repeatedly reported for monosaccharides, polysaccharides, and exopolymeric substances (EPS), pointing toward additional transporter route rather specific to dissolved organic carbon than to Fe. Because EPS can attach to cell surface, they also have the potential to increase Fe diffusive supply at the cell surface (*16*, *50*). However, the mechanism at play is still not understood.

When considering each station separately, we observed that the Fe uptake rates by *P. antarctica* show some relationship with increasing in situ dFe (but no clear relationship with Fe′) at certain stations. In addition, different linear trends were observed from station to station (Fig. 4). However, when all samples are considered together, the correlation between dFe or Fe′ concentration and Fe uptake rates is weak (r = 0.41 and 0.18 for dFe and Fe′, respectively). This suggests a high disparity between samples in terms of bioavailability, which cannot be solely attributed to differences in dFe or Fe′ concentrations. This finding is clearly illustrated by upper ocean data (0 to 100 m) where similar dFe concentrations (0.04 ± 0.02 nmol/liter, n = 20) were found; yet markedly, Fe uptake rates varied by three orders of magnitude (Fig. 4). Notably, station TMR12 also showed intriguingly low Fe uptake rates (2.2 ± 1.5 × 10^{-22} mol Fe cell^{-1} hour^{-1}, n = 27 all replicates included). Last, all values falling above the boundaries of 50% bioavailability belong to stations that were directly under the influence of a glacial or sediment dFe source, as inferred from distinct δ^{56}Fe signatures at these stations [TMR11, TMR13, and TMR14; Fig. 4A; (*9*)].

dFe bioavailability cannot be inferred from conventional Fe speciation measurements

To better understand the large range observed in dFe bioavailability among our samples, we further explored what factors are correlated in our dataset. The magnitude, direction, and significance of the correlation between selected variables are summarized in Fig. 5. Overall, we did not obtain any significant correlation between Fe uptake by *P. antarctica* and additional variables listed in table S2 other than a spurious correlation with dFe concentration (computationally related; see Material and Methods for Fe uptake calculation). However, we did obtain a significant negative correlation between dFe bioavailability and eHS concentrations (r = −0.33, P = 0.04, n = 33). The absence of correlation between depth and Fe uptake rates further supports the argument that dFe bioavailability was not primarily driven by dFe concentration but instead was more strongly related to the nature of Fe sources and ligands. Intriguingly, in the first ever direct comparison of dissolved δ^{56}Fe and Fe-binding ligands, we found a negative correlation between L_T concentration and δ^{56}Fe (fig. S2) but a positive correlation between δ^{56}Fe and eHS (Fig. 5A). To investigate this relationship between L_T and δ^{56}Fe further, we also used principal components analysis (PCA; Fig. 5B).

The two first principal components (PCs) explained, respectively, 36.5 and 24.1% of the total variance. The first component (PC1) separated the variables in two categories. Negative values of PC1 correspond to TPZT and eHS concentrations, and positive values were related to all other variables. The variables contributing mainly to PC1 are dFe concentration and δ^{56}Fe signature. The second component (PC2) mainly separated ligands from Fe speciation and Fe uptake. The variables contributing mainly to PC2 are total ligands, TPZT, and eHS concentrations. These results, descriptive as they are, open up several lines of discussion, including the

Table 1. Summary of Fe speciation and ligands properties. Range of dFe concentrations and Fe speciation results, including total Fe-binding organic ligand concentrations (L_T), log-conditional stability constants ($logK'_{Fe'L}$), and concentrations of carbohydrates (TPZT) and eHS (expressed in equivalent of terrestrial standard SRFA). Data represent ranges for Fe speciation from surface down to 500-m depth.

	Station	Latitude (°S)	Longitude (°E)	dFe (nmol/liter)	Fe′ (pmol/liter)	L_T (nmol/liter)	$LogK'_{Fe'L}$	TPTZ (µmolC/liter)	eHS (µg/liter eq. SRFA)
Polynya	**TMR11**	−67.1036	144.9204	0.036 to 0.410	0.32 to 6.76	0.99 to 6.22	10.3 to 11.6	1.36 to 8.01	20 to 42
	TMR12	−67.1895	145.7209	0.042 to 0.300	0.71 to 4.49	1.35 to 8.15	10.2 to 11.3	6.73 to 17.5	4 to 329
Islands	**TMR13**	−65.9917	159.0120	0.028 to 0.387	0.01 to 0.53	6.83 to 13.7	10.7 to 12.4	4.14 to 9.65	11 to 183
	TMR14	−67.2897	163.5360	0.085 to 0.456	0.06 to 2.65	3.97 to 15.7	10.4 to 12.0	2.82 to 9.65	17 to 268
Open ocean	**TMR15**	−67.0999	167.3602	0.024 to 0.585	0.16 to 0.50	6.27 to 7.89	11.0 to 11.7	3.52 to 6.28	14 to 230
	TMR16	−71.6993	−143.983	0.023 to 0.294	0.11 to 2.66	0.92 to 2.30	10.5 to 12.1	1.87 to 2.77	7 to 117

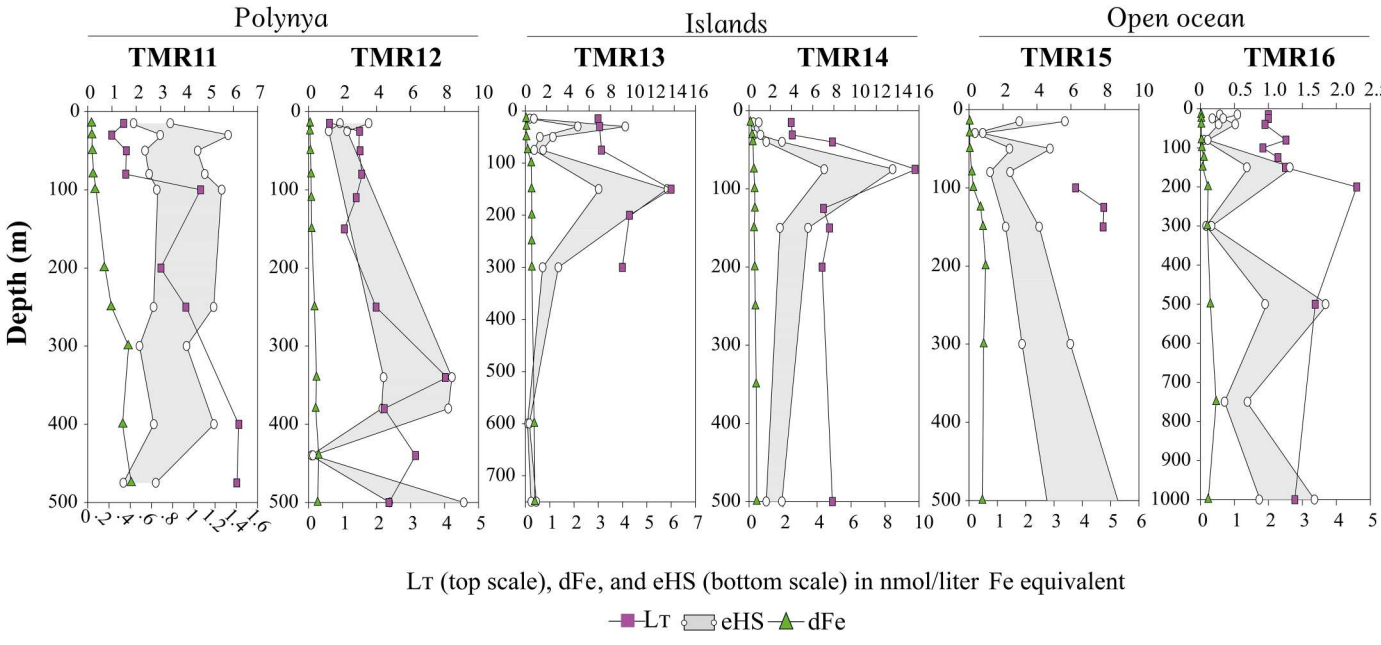

Fig. 2. Combined data for eHS, dFe, and L_T. Individual profiles for stations TMR11 to TMR16 of dFe (green triangle) and total Fe-binding organic ligand (L_T, purple square) concentrations with an envelope (gray) for eHS, encompassing the maximum and minimum Fe-binding capacities reported for terrestrial International Humic Subtances Society (IHSS) standards. Each plot represents one measurement from seawater samples collected in the Mertz glacier polynya (TMR11 and TMR12), downstream of the Balleny islands (TMR13 and TMR14) and in the open ocean near the Balleny islands (TMR15) or the Ross Sea (TMR16).

role of biologically mediated molecules acting as Fe-binding ligands (see Discussion).

DISCUSSION

Using metrics of dFe bioavailability for ocean-wide comparisons

Despite the conceptual utility of the term bioavailability, many poorly constrained factors are involved in its determination. In the natural environment, light, temperature, Fe speciation and kinetics, microbial interactions, and adaptations are all intertwined into its definition, and it is challenging to tease apart the role of each process separately. Here, we aimed to overcome this complexity by using one ecologically relevant phytoplankton species (*P. antarctica*) to enable a unique diagnostic of dFe bioavailability in the SO and to investigate the connection between assessed dFe bioavailability and in situ Fe speciation.

To compare our results with other studies that used different phytoplankton species, the apparent Fe uptake rate constant $k_{in\text{-}app}$

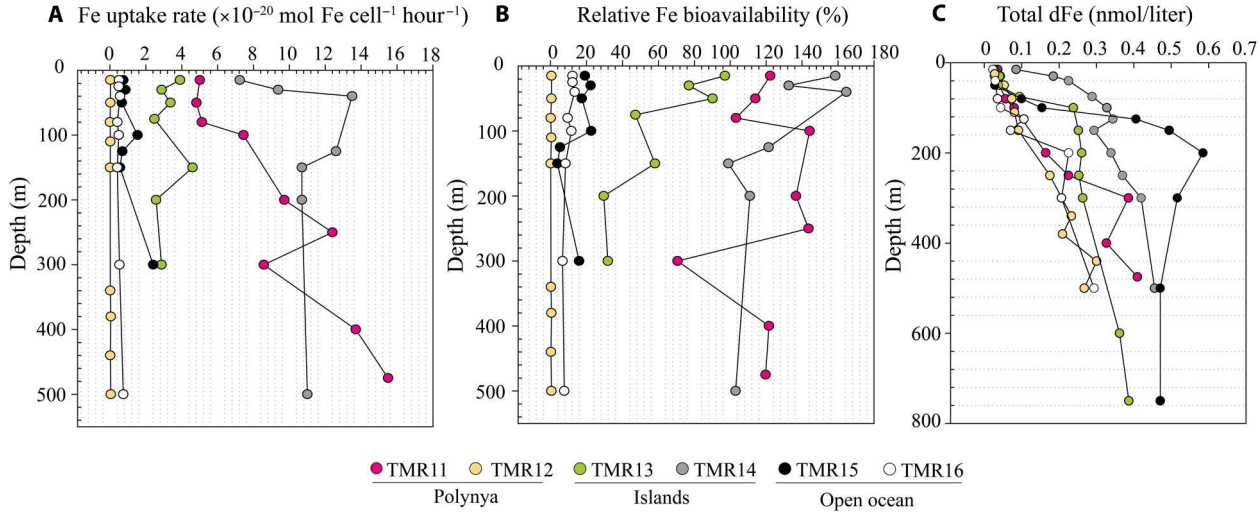

Fig. 3. Range of bioavailability for dFe complexed with natural ligands. Profiles of Fe uptake rates by *P. antarctica* (**A**) compared to estimated uptake of inorganic Fe (Fe′) (**B**) as a proxy of dFe bioavailability and to total dFe concentration (**C**).Each dot represents the average value of three independent replicates from samples collected in the Mertz glacier polynya (TMR11 and TMR12), downstream of the Balleny islands (TMR13 and TMR14), and in the open ocean near the Balleny islands (TMR15), or the Ross Sea (TMR16). SDs were omitted here to allow better visualization but are given in table S1.

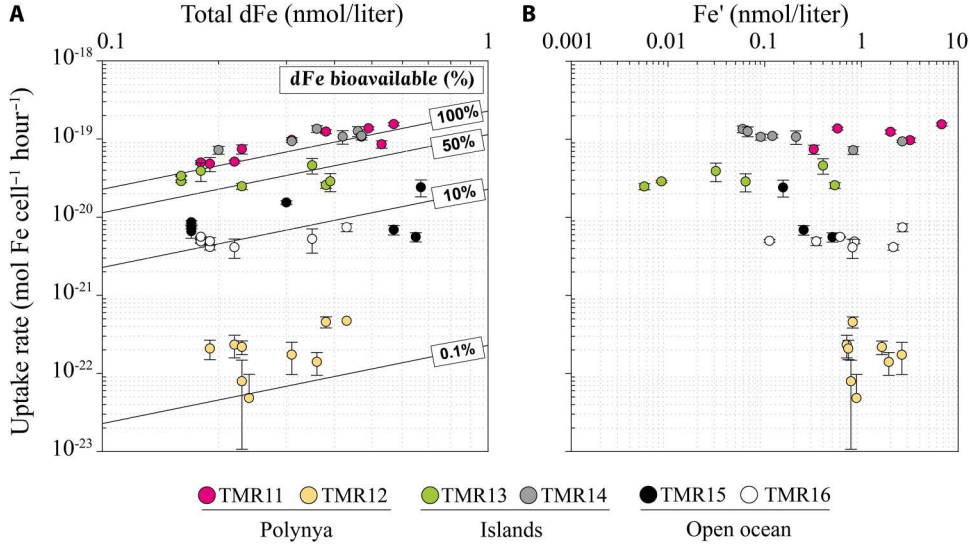

Fig. 4. Relationship between dFe bioavailability and dFe/Fe′ concentrations. Fe uptake rates by *P. antarctica* as a function of total dFe (**A**) and Fe′ concentration (**B**). Data are presented on a logarithmic scale.

(*36*) was calculated as

$$k_{\text{in-app}}(\text{liter}\cdot\text{cell}^{-1}\cdot\text{day}^{-1}) = \frac{\text{Fe uptake rate}\ (\text{molFe}\cdot\text{cell}^{-1}\cdot\text{day}^{-1})}{\text{dFe conc.}(\text{nmol}\cdot\text{liter}^{-1})}$$

The $k_{\text{in-app}}$ calculation implies that Fe-limited phytoplankton cells access Fe primarily from the ligand-bound pool, which was the case in our experiments (see Materials and Methods). These $k_{\text{in-app}}$ values were further normalized to the cell surface area (S.A.) of *P. antarctica* (S.A. = 28.71 μm^2 per cell). To facilitate comparison with previous investigations, we combined our average dFe bioavailability proxy ($k_{\text{in-app}}$/S.A.) calculated per station [using the data from (*37*)], with the "dFe bioavailability envelope" proposed by (*36*). This envelope is delimited by the highly bioavailable inorganic Fe′ as its upper boundary and the very bio-unavailable Fe complexed to the strong siderophore desferrioxamine B (DFB) as its lower boundary (Fig. 6). We excluded station TMR12 from the following analysis because extreme values measured at this station may hinder comparisons across studies. On average, the $k_{\text{in-app}}$/S.A. (1.30×10^{-10} liter μm^{-2} day^{-1}) was 18-fold lower than for Fe′ (2.4×10^{-9} liter μm^{-2} day^{-1}) and 54-fold higher than for the FeDFB complex (2.4×10^{-12} liter μm^{-2} day^{-1}). It was also 3.4-fold higher than the only value reported so far for the open SO [3.8×10^{-11} liter μm^{-2} day^{-1}; (*37*)]. This observation highlights that dFe bioavailability can be extremely variable. There is a clear distinction between open ocean, which are equivalent to other

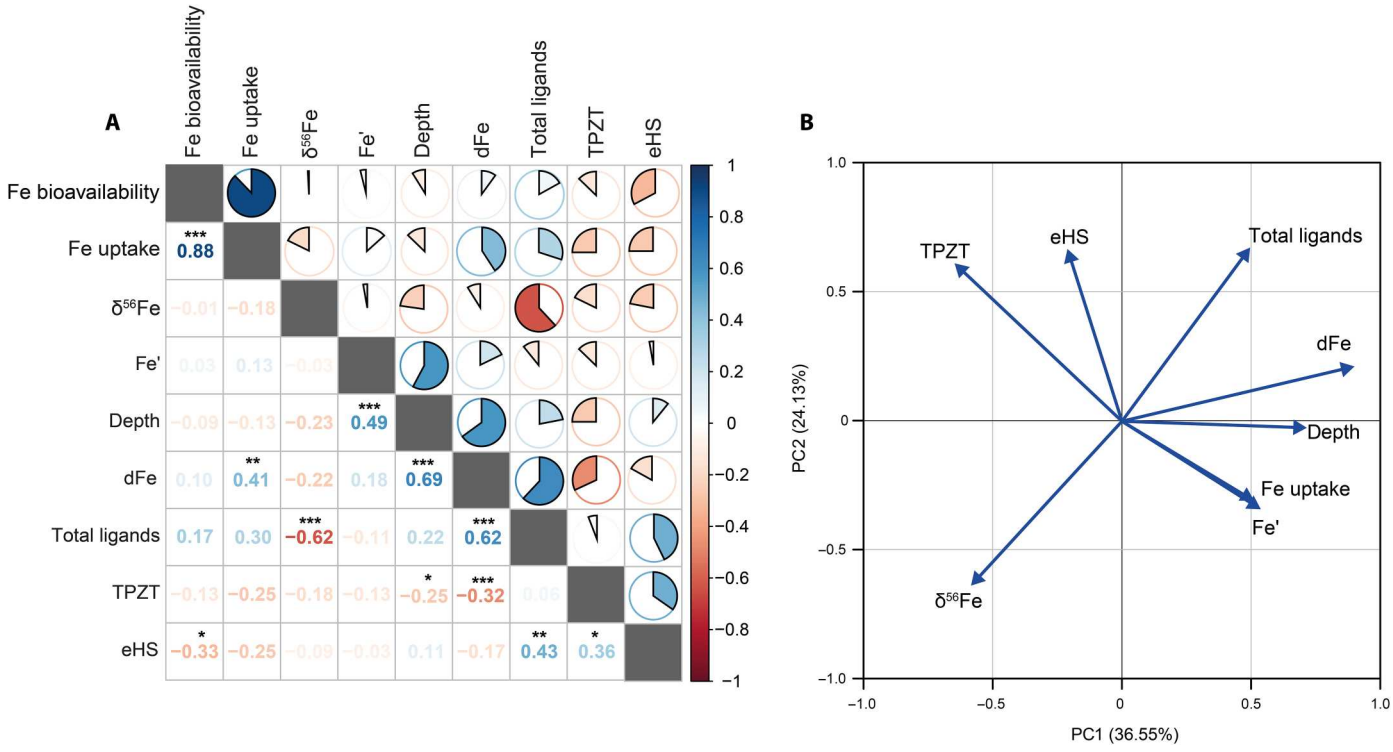

Fig. 5. Drivers of dFe bioavailability. (**A**) Correlation matrix between Fe speciation, dFe bioavailability, and Fe uptake calculated using the Pearson product moment correlation. Correlation coefficients (*r*) are represented in gradient color, and blue and red indicate *r* values above and below 0, respectively. Significant relationships between the two variables (pairs with *P* values smaller than 0.05) are annotated with stars (*$P < 0.05$, **$P < 0.01$, and ***$P < 0.001$). Summary of variables presented in the table below. (**B**) PCA correlation of Fe uptake, Fe chemistry, and ligands. Blue arrows represent the projection of the descriptors into the two first PC plans. The two first PCs explain respectively 36.55 and 24.13% of the total variance. Normality was verified using Henze-Zirkler test.

ocean basins, and near-source stations, which have an order of magnitude higher bioavailability than open ocean, even compared to previous estimates from (*37*) in the Drake passage (Fig. 6). However, it is also noteworthy that the two stations within the Mertz glacier polynya (TMR11 and TMR12) exhibited such high differences in bioavailability despite similar dFe, δ^{56}Fe, and relative proximity to Fe source (*9*). Hence, the consensus of a nearly constant dFe bioavailability (*37*) does not apply to these SO samples. Because of the limited amount of data in the different ocean basins and the focus of this study on naturally fertilized sites, it remains to be determined whether this large variability is a particular feature for the SO.

Examining the dFe bioavailability proxy: Limitations and implications

In the natural environment, the concept of bioavailability is not separated from, but encompasses, ecological interactions and specific biological adaptations. We approached this complexity with the idea that a single model organism can be used to simplify the biological components and better address the chemical ones. The wide range in the dFe bioavailability proxy (Fig. 6) for *P. antarctica* demonstrates that chemistry, beyond biology, influences the bioavailability of Fe in the SO. However, we cannot ignore that biodiversity would influence these estimates of dFe bioavailability in situ and that the complexity of the system as a whole goes far beyond the responses of a single strain. Uptake rates normalized to dFe concentration as a function of cell S.A. indirectly account for the number of transmembranar proteins, but the current proposed Fe bioavailability model may further be complicated when considering various transport systems. In the bioavailability model, all Fe forms are taken up as Fe^{2+}, implying that a limiting step is the rate of the formation of Fe^{2+}, which, for instance, can be aided by the presence of extracellular reductases (*36*, *49*). The transcriptomic response of this particular strain of *P. antarctica* to Fe limitation did not show gene regulation for ferric or ferrous ion transporters (*51*); however, other studies have revealed previously unknown Fe-responsive transcripts for Fe′ in diatoms (*52*, *53*). Consequently, we emphasize that these results cannot be easily extended to broader calculations, such as dFe residency time. Therefore, caution must be taken when generalizing these results, and further investigations are needed to determine the broader applicability of our findings to other regions of the SO.

The influence of Fe sources on dFe bioavailability to *P. antarctica*

The respective location of the stations provides a balanced representation of the upper ocean in naturally fertilized area of the SO, with different potential sources of Fe. Overall, our work indicates that dFe bioavailability is higher close to dFe sources than in the open waters of the SO, particularly, close to glacial meltwaters. However, we also note that the two stations located in the Mertz glacier polynya, while showing similar dFe, δ^{56}Fe, and Fe′ ranges, have astonishingly different uptake rates (10^{-22} and 10^{-19} mol Fe^{-1} cell $hour^{-1}$) and dFe bioavailability relative to Fe′ (<1%

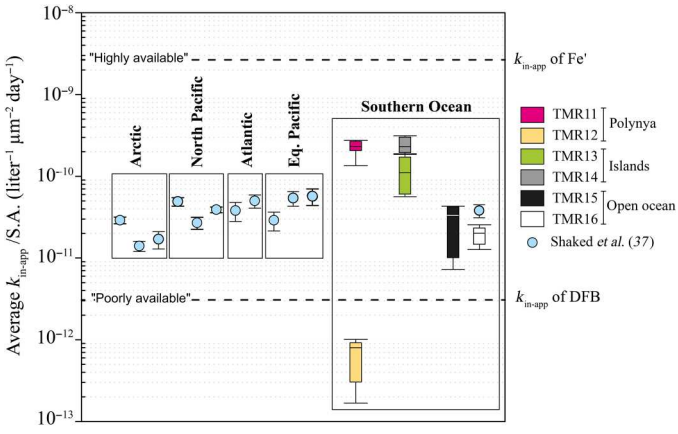

Fig. 6. Combined results of the Fe-substrate bioavailability as Fe-uptake rate constant normalized per surface area (k_{in-app}/S.A.). The bioavailability envelope's boundaries are delineated by dotted lines, with unchelated inorganic Fe (Fe′) as its upper boundary and FeDFB as its lower boundary. Each box plot represents a different station from this study, while circles represent measurements from (*37*). The line across the boxes represents the median. The ends of the boxes define the 25th and 75th percentiles, and error bars define the 10th and 90th percentiles (data pooled from all depths). Literature data: Arctic: Baffin Bay (37 m), Canadian Arctic archipelago (44 m), and Beaufort Sea (10 m); North Pacific: Line-P stations P16 (25 m), P20 surface (25 m), and P20 depth (800 m); SO (Drake Passage, 100 m); Atlantic: Gulf of Mexico (2 m), GEOTRACES GA03 Atlantic Zonal Transect (100 m); equatorial Pacific (Eq. Pacific): GEOTRACES GP16 Oxygen Depleted Zone (20 m), surface (2 m), and depth (3000 m) (*35*). From this study, all stations are located in Antarctic waters (south of 65°S) and grouped/colored according to their location; Polynya: TMR11 (15 to 475 m) and TMR12 (15 to 500 m); Islands: TMR13 (15 to 300 m) and TMR14 (15 to 500 m); Open ocean: TMR15 (15 to 300 m) and TMR16 (15 to 500 m). Data are presented in log scale.

versus >100%). Yet, mechanistically, this is consistent with transformations of nanoparticulate Fe oxyhydroxides, which are known to be highly soluble (*54*, *55*) and highly reactive, as shown by their fast rates of transformation (*54*). More attention is required to understand the dynamic and contrasted situation within these oceanographic features, especially the Mertz glacier polynya, which is one of the most productive polynyas in Antarctica (*56*).

Stations TMR13, TMR14, and TMR15 were all located in the vicinity of the heavily glaciated Balleny islands of volcanic origin, but were likely affected by different Fe sources. Stations TMR13 and TMR14 exhibited shallow ferriclines (40 and 100 m at TMR14 and TMR13, respectively) than average values usually observed in this region (200 m), which is indicative of natural Fe supply from the islands (*9*, *46*). On the east side of the Balleny islands (TMR15), however, elevated dFe and L_T concentrations and a shift of Fe isotopic signature to negative values (from near 0 at 300 m to near −2‰ at depth) were clearly visible (fig. S1), which may indicate a hydrothermal input (*57*). Hydrothermal vents were recently identified as an important source of bioavailable dFe (*58*) that potentially triggers massive blooms of *P. antarctica* in SO surface waters (*42*). At station TMR15, all depths averaged, the dFe bioavailability proxy (k_{in-app}/S.A.) was 8.4-fold higher than for FeDFB but respectively 2 to 10 times and 5 to 29 times smaller to what was measured at TMR13 and TMR14. If TMR15 was indeed under the influence of hydrothermal vents, then this suggests that dFe from this potentially hydrothermally affected seawater was more available to phytoplankton than model strong Fe-siderophore complexes but also less bioavailable than dFe supply's origin is sedimentary or glacial.

Driving factors of dFe bioavailability: Fe′, ligands, and Fe sources

Moving from an average value at each station to individual depths, another remarkable result is the highly contrasting range of dFe bioavailability with depth, especially at the near-source stations (Fig. 3). Considering that k_{in-app}/S.A. cannot be influenced by the presence of different organisms nor by variations in biomass in our study (see Material and Methods) nor by the release of Fe′ through photodegradation of Fe-ligand complexes (*47*, *48*, *59*), this high variability was unexpected. The possible mechanisms driving this variability in k_{in-app}/S.A. are explored below.

Although Fe chemical speciation influences dFe bioavailability, our analysis failed to identify a consistent link between Fe uptake rates and dFe concentration, eHS or L_T, contrary to our expectations. Our dataset showed that both eHS and TPZT concentrations were anticorrelated with estimates of dFe bioavailability, suggesting that neither is the sole source of bioavailable Fe (Fig. 5). We found significant correlations between Fe uptake rates and L_T [coefficient of determination (r^2) = 0.65, P = 0.001, n = 14] or dFe concentrations (r^2 = 0.72, P < 0.001, n = 15) only at stations TMR11 and TMR14. These two stations also exhibited the highest dFe bioavailability of all (70 to 165%), which can be attributed to their proximity to local Fe sources. However, they did not show the highest Fe′ or eHS concentration, suggesting that Fe source matters in defining its bioavailability.

While there is no strong relationship between Fe uptake rates and Fe′ concentrations when considering the entire dataset, certain stations display correlations (Fig. 4), implying that Fe uptake may partly be controlled by Fe′ diffusive flux and Fe-ligand dissociation kinetics. In seawater, most of the dFe is bound to organic ligands, while only a small fraction exists as inorganic species. This Fe′ is small enough to passively diffusive through general or ion-selective porin, allowing for cellular Fe′ uptake by molecular diffusion (*20*, *38*). The supply rate of Fe′ in surface waters is usually believed to be too slow to account for observed Fe uptake rates, indicating the need for phytoplankton to access organically bound Fe species (*50*, *60*–*62*). Here, we estimate that the supply of Fe′ due to the dissociation from Fe-ligand complexes could effectively meet the Fe demand by phytoplankton in ~80% of our incubations (table S1). Therefore, while Fe′ levels as a "snapshot concentration" cannot explain measured Fe uptake rates (Fig. 5A), the rate of continuous Fe′ supply by ligand dissociation may in fact play a substantial role in controlling dFe bioavailability. This finding agrees with previous observations that Fe′ may represent a significant pool for the Fe biological requirement in many areas of the SO (*15*, *41*).

A limited role of Humics in Fe biogeochemistry in the SO?

dFe has been shown to covary with eHS in other ocean basin regions (i.e., Atlantic and Pacific oceans), but low Fe-binding capacities of eHS in samples from the SO have been reported (*29*). Our observations give further insight on the potential role of eHS in the SO, indicating that the lack of relationship between dFe and eHS may be a particular feature for the SO (Fig. 5A). We found not only that the average Fe-binding capacity of eHS compounds was well below the L_T measured for most samples in our study (Table 1) but also that

the relative eHS contribution to Fe-binding ligands (36 ± 40%) was much lower than previously reported (191 ± 99.7%) for other ocean basins [northeast Pacific and the northwest Atlantic from (*29*)]. In our case, despite the clear contribution of eHS to L_T (indeed, eHS shows a positive correlation with L_T; Fig. 5), other compounds are contributing to the bulk of ligands and may play a bigger role in dFe bioavailability. For instance, in contrast with eHS, biologically mediated ligands (e.g., TPZT) were significantly correlated with dFe concentration in our dataset but not with L_T. This points toward a disproportionate role of biologically mediated ligands on Fe biogeochemistry (*12*, *63*) relative to their contribution to the total ligand pool in the SO. It highlights the significance in constraining regulations of dFe bioavailability and not simply dFe or Fe′ and L_T. This also supports recent results indicating that Fe recycling within the microbial loop [aka "ferrous wheel" (*64*)] is highly efficient in the SO, helping to increase the residence time of dFe in surface waters, and that particle-associated microbial respiration generates weak (L_2) ligands that form bioavailable FeL complexes (*63*).

Linking δ^{56}Fe, dFe bioavailability, and Fe-binding organic ligands

Despite being a key aspect for global biogeochemical modeling of dFe and δ^{56}Fe (*2*, *65*, *66*), the character, sources/sinks, binding strength, and Fe isotope fractionation factors of organic ligands remain poorly constrained (*67*). Elevated δ^{56}Fe values can be driven by biological uptake (*68*, *69*), rapid recycling (*70*), and/or complexation with low–molecular weight or strong Fe ligands (*71*, *72*). However, only a couple of laboratory studies have linked δ^{56}Fe signature directly to the presence and binding properties of possible organic ligands (*73*, *74*), and fractionation during complexation has not been measured for natural open ocean ligand assemblages. To date, the first ocean biogeochemical models have assumed generic fractionation factors ($\triangle\delta^{56}$Fe) of +0.6‰ for complexation (ligands-dFe) and −0.5‰ for biological uptake (phytoplankton-dFe) based on laboratory work or inferred from limited open ocean δ^{56}Fe data (*9*, *66*, *67*, *70*).

Our coupled dataset of Fe-binding ligands, dFe bioavailability, and δ^{56}Fe offers a chance to tease apart these processes further. We found a negative correlation between dissolved δ^{56}Fe and total ligand concentrations ($r = -0.62$, $P < 0.0001$, $n = 38$; Fig. 5), which might suggest against a role for complexation in driving dissolved δ^{56}Fe toward higher values, in contrast to previous assumption (*73*, *74*). However, this outcome is not entirely unexpected. Different ligands are anticipated to have different binding strengths and fractionation factors, rendering the concentration of the total pool not be the most relevant parameter, as demonstrated above for dFe and bioavailability. Further, if the isotopically heavy Fe is bound to strong Fe-binding ligands, which would have greater isotopic fractionation factors (*73*, *74*), then we might expect this dFe to have lower effective bioavailability compared to Fe′ or dFe bound to weaker ligands.

Overall, our data demonstrate a link between δ^{56}Fe, Fe uptake, and ligands, thus reinforcing the utility of isotopic analysis as a tool to identify Fe sources. However, understanding of the processes that control δ^{56}Fe is complicated by competing processes and sources across the SO, with (*9*) finding that dataset for surface waters could not easily be described by a single fractionation factor. The only exception to this finding was for sites within the Mertz glacier polynya (TMR11 and TMR12), where δ^{56}Fe and dFe in the top 200 m could be described with a closed Rayleigh fractionation factor α of 0.999 (*9*), suggesting that a single process dominated the isotopic fractionation at these locations. This was attributed to removal of light Fe into phytoplankton, perhaps in a single phytoplankton bloom, also consistent with an α of 0.999 inferred for uptake in an SO eddy (*9*, *70*). In addition, the low surface dFe could be attributed to biological activity, considering the lower macronutrient concentrations and the proximity to a dFe source (*9*, *46*). In situ measurements also confirmed that surface waters were characterized by elevated phytoplankton biomass (Chl a) and high net primary production (O_2/Ar) at the time of sampling (*75*). In this study, we further identify a pronounced trend between Fe uptake rates by *P. antarctica* and dissolved in situ δ^{56}Fe at TMR11 (fig. S3). A similar relationship between ambient dissolved δ^{56}Fe and Fe uptake was also found for dissolved δ^{114}Cd and Fe uptake at the same station (fig. S4) (*9*), suggesting that δ^{114}Cd may be a tracer of nutrient uptake (*76*).

Given that all Fe species in the dissolved phase are currently considered to be equally bioavailable in most ocean biogeochemistry models (*3*, *77*), our findings emphasize the need to reassess which criteria of ambient Fe are central to estimating dFe bioavailability and, ultimately, primary production in the SO. Despite this, many studies have demonstrated the usefulness of dFe concentrations as an operational metric for bioavailable Fe concentration. This raises questions about the influence of biodiversity, connectivity, adaptive capacity, and the scale and frequency of Fe inputs on dFe bioavailability. To broaden our perspective, we recommend further assessment of the importance of eHS in the SO and the evolution of this bioavailable fraction during transport, aging, and recycling from local point sources. In the present stage of our knowledge, it is also unknown what modulates Fe-binding ligands and Fe isotopes in concert. As a first step, it is necessary to get a nuanced understanding of the processes that lead to isotope fractionation. This could be achieved by determining Fe isotopic composition of phytoplankton in cultures exposed to different Fe-ligand complexes. Mass balance calculations can further be used to probe fractionation steps during biological uptake, thereby offering a new window to distinguish between different biotic and abiotic processes. Because the SO carries long-term climate trends in Fe-fertilized areas, these data draw attention to oversimplification of the internal Fe and C cycles in this region. This should not be ignored, particularly in the context of Fe dispersal praised by geoengineering proposals to generate CO_2 sink.

MATERIALS AND METHODS

Oceanographic settings

Six different locations were sampled for vertical profiles (0- to 500-m depth) south of the southern ACC boundary (Fig. 1) as part of the Antarctic Circumnavigation Expedition (GEOTRACES Compliant Cruise GSCo1; *R/V Akademik Tryoshnikov*, January to March 2017). Two stations were within the Mertz glacier polynya (TMR11 and TMR12), two stations were sampled downstream (TMR13 and TMR14) and one upstream (TMR15) of the volcanic Balleny islands, while one station was located in the open waters of the Ross Sea (TMR16).

TM sampling procedure and Fe speciation analysis

All culture ware and material used during this study were trace-metal (TM)–clean following GEOTRACES protocols (*78*), and all sample manipulations were conducted in a TM-clean laminar-flow hood (HEPA, class 100) or in a clean room using TM clean techniques. Solutions were systematically prepared using analytical grade chemicals (Sigma-Aldrich, Buchs, Switzerland) and Milli-Q water unless otherwise specified. In details, when first used, polycarbonate (PC) bottles were rinsed five times with Milli-Q water and subsequently soaked for 1 week in a large container filled with Citranox (2% diluted in Milli-Q water at ambient temperature), so that the inside and outside of the bottles were in contact with the detergent. After 1 week, PC bottles were abundantly rinsed for several minutes under deionized water and then rapidly rinsed with Milli-Q water. They were then soaked in 10% HCl for 4 to 5 weeks, followed by rinsing seven times with Milli-Q water. PC bottles were then left in a Milli-Q water bath for 1 week. The same decontamination process was used for PC bottles after use with ^{55}Fe, except that RBS25 was used as a detergent. Between experiments with similar low dFe concentrations, the bottles were washed with one rinse of Milli-Q water, soaked in RBS25 for 24 hours, soaked in a 10% HCl bath for 1 week, and rinsed seven times with Milli-Q water. The efficiency of removing ^{55}Fe was regularly verified. We also paid attention to unwanted ^{55}Fe adsorption to the plastic walls in our calculations. To do this, we systematically sampled 1 ml from each bottle incubation for ^{55}Fe measurement before the addition of cells and at the end of the incubation. We found that a relatively low percentage of ^{55}Fe was adsorbed onto the plastic surface (1 to 5%).

Sampling

For the determination of Fe speciation and for Fe uptake experiments, we sampled water from the depth profiles. In total, 47 seawater samples from the six stations in the SO (Fig. 1) were collected, spanning the uppermost 500 m of the water column, with a particular focus on high depth resolution in the top 200 m. At each station, the deployment of a conductivity-temperature-depth (CTD) was performed just before the deployment of the rosette to guide the sampling depths chosen for our analysis. Sampling was then conducted using an autonomous TM rosette (model 1018, General Oceanics, USA) equipped with acid-cleaned Teflon-coated 10-liter Niskin-X bottles, and seawater was directly filtered onboard into in a clean container—with high efficiency air particulate filter system—through 0.2-μm acid-cleaned capsule filters (AcroPak 200, Pall). Seawater samples were subsequently stored into 1-liter acid-cleaned low-density polyethylene Nalgene bottles, frozen at −20°C, and shipped to home laboratories for analyses. Filtered samples from the same Niskin-X bottles were taken by other groups for analysis of dFe and δ^{56}Fe at each depth (*9*, *46*).

Fe chemistry and analysis of organic ligands

The main parameters acquired via ligand exchange–adsorptive cathodic stripping voltammetry are total ligand (L_T) concentrations and their conditional stability constants for Fe ($\log K'_{Fe'L}$). Ligands with a $\log K'_{Fe'L} > 12$ are operationally assigned as "strong" ligands, while those with a $K'_{Fe'L} < 12$ are considered as "weak" ligands (*18*). A full description of the method is provided in (*21*). Briefly, 10-ml aliquots of the filtered seawater samples were transferred to acid-cleaned 15-ml low-density polyethylene bottles (Nalgene, Thermo Fisher Scientific). Tubes were preconditioned with water collected from the same area and the planned Fe and additions. Each aliquot was then buffered to pH 8.2 with 1 mol/liter borate buffer, and after an equilibration time of 1 hour at room temperature, a solution of 5 μmol/liter of the competitive ligand salicylaldoxime (98% Acros Organics, Thermo Fisher Scientific) was added. Aliquots were analyzed the next day following an equilibration time of at least 12 hours.

Hydrolysable carbohydrates were quantified by 2,4,6-tripyridyl-*s*-triazine (TPTZ) spectroscopy using the method in (*79*, *80*). Hydrolysable carbohydrates (later referred as TPZT from the analytical methodology used) is part of the labile pool of dissolved organic carbon, and these data are used to explore the nature of Fe ligands. This technique is based on the reduction of Fe^{3+} into Fe^{2+}, which reacts with TPTZ forming a blue complex absorbing at 595 nm. D-glucose was used as a standard. The instrumental detection and quantification limits were 2.46 and 4.29 μmolC/liter, respectively. eHS concentrations, abbreviated eHS and expressed in microgram equivalent per liter using terrestrial standards from the Suwannee River (SRFA), were determined by electrochemistry following standard additions of SRFA [standard 1. IHSS, (*21*)]. TPTZ and eHS are considered as weak ligands.

Auxiliary parameters analysis

Temperature and salinity were obtained from calibrated CTD (SeaBird SBE11, General Oceanics, Miami, FL, USA) mounted on the TM rosette. A body of chemical and biological parameters was tested for correlation with our analyses of Fe uptake rates (table S2). Full dataset of these parameters and detailed methods can be found in (*9*, *46*, *57*, *81*) for nutrients, TMs, and isotopes and (*75*) for biological parameters.

Estimating the contribution of humic substances to the in situ ligand pool

Similar to (*29*), the contribution of humic substances to the pool of in situ ligands was estimated using in situ eHS measurements as the amount of Fe-binding humic substances present. As two borderline situations, humics were considered either as weak (SRFA, 16.7 nmol of Fe mg^{-1}, $\log K_{Fe'L} = 10.6$) or strong ligand [SRHA, 31.9 nmol of Fe mg^{-1}, $\log K_{Fe'L} = 11.1$; (*30*)]. By using the total Fe-binding capacities of humic substances, one can estimate their saturation level with Fe and convert eHS into maximal Fe-binding ligand equivalent. However, this maximal amount represents an upper limit, assuming that all dFe will bind to this type of ligand and not accounting for any side reactions with other trace elements capable of binding to these ligand types. Moreover, it assumes that marine eHS all behave as SRFA and SRHA. By comparing concentrations of estimated maximal ligand equivalent with in situ ligands, one can derivate the maximal contribution of humics [Humic Acid (HA) and Fluvic Acid (FA)] to the in situ ligand pool. Here, we used ligand data instead of dFe data as in (*29*), which is more relevant as in situ ligands generally exceed dFe concentrations.

Laboratory-based biological Fe uptake

Model organism: P. antarctica

The Prymnesiophyceae *P. antarctica* (strain CCMP3314, isolated at 68°39′S, 72°21′E) was selected to determine dFe bioavailability in bioassays. We did not observe colony formation with this strain, although other strains of *P. antarctica* (such as CCMP1871 and

CCMP1374) can shift from flagellate cells to most the of colonial cells under Fe-replete conditions (*82*). This strain is also quite stable in its physiology as its measured growth and particulate organic carbon production rates are very similar across various experiments (*51*, *83*) and easy to manipulate (e.g., no EPS formation), making it the perfect candidate as a model organism. For the purposes of this study, single cells of *P. antarctica* were maintained in natural seawater media prepared from 0.2-µm filtered seawater collected during the expedition PS97 (*R/V Polarstern PS97*, 25-m depth, 60°S, 66°W, 2 to 3 March 2016). This natural seawater had a background concentration of 0.74 nmol/liter dFe (with 1.45 pmol/liter Fe′), 1.67 nmol/liter total ligands, and was naturally enriched with other essential trace elements such as zinc and cobalt. We kept our cultures in the exponential growth phase by regular transfers into the medium freshly amended with 0.3 mmol/liter $NaNO_3$, 10 µmol/liter $NaH_2PO_4.2H_2O$, 0.1 mmol/liter $Na_2SiO_3.5H_2O$ (chelexed stock solutions; Chelex-100 BioRad, Cressier, Switzerland), and 1.27 nmol/liter Se (inductively coupled plasma standard). Microwaving was used for sterilization (four consecutive cycles of heating-cooling for 5 min) and vitamins (0.3 µmol/liter thiamine HCl, 2 nmol/liter biotin, and 0.4 nmol/liter vitamin B12, final concentration) were added at room temperature. Before cell transfer, medium was equilibrated at 4°C for 24 hours.

Growth and physiological condition

P. antarctica monocultures were grown at 4°C, with 50 µmol quanta m^{-2} s^{-1} supplied by cool white fluorescent lights under a 12:12-hour light:dark cycle. The presence of unwanted prokaryotes and eukaryotes were not detectable in the cultures after examination using dual epifluorescence 4′,6-diamidino-2-phenylindole staining (OLYMPUS BX61, Volketswil, Switzerland). Fe limitation was verified by regular measurements of the maximum photochemical efficiency of photosystem II (termed *Fv*/*Fm*), commonly used as an index of nutrient status under Fe stress (*84*). *Fv*/*Fm* was determined on the basis of variable Chl a fluorescence using the fast repetition rate fluorometer FastOcean PTX coupled to a FastAct base unit (Chelsea Technologies). The FastAct base unit allows the circulation of water around the sample to maintain incubation growth temperature (4°C) during the measurements. Before analyses, cells were transiently acclimated to dark for 30 min. In our experiments, *Fv*/*Fm* was at a low level of 0.3, which further confirmed Fe limitation in cells. Cell surface area (S.A.) was determined in vivo in preconcentrated samples mounted in microscope slides using the microscope OLYMPUS BX61 (Volketswil, Switzerland) coupled with a Photometrics CoolSnap FX cooled charge-coupled device camera. Images were analyzed with the imaging software CellSens to determine cell dimensions, counting about 300 cells.

Probing dFe bioavailability to P. antarctica in natural seawater samples

The bioavailability of dFe in each seawater sample was estimated on the basis of intracellular Fe uptake rates of *P. antarctica*. First, seawater samples were allowed to slowly thaw at 4°C in the dark and split into four subsamples (150 ml, three biological replicates, and one blank control) in TM-cleaned 250-ml PC bottles. All subsamples were subsequently spiked with the radiolabeled ^{55}Fe (inorganic as $FeCl_3$, specific activity of 80.85 mCi mg^{-1}; PerkinElmer) that was added as a low amount (0.15 ± 0.02 nmol/liter, n = 188 subsamples of natural seawater) so as not to exceed solubility limit of Fe(III) at 4°C (*85*). The inorganic ^{55}Fe was allowed to equilibrate (with the mixture of natural ligands present in the natural samples) at the experimental temperature of 4°C for 24 hours and in total darkness to avoid photodegradation. To begin the experiment, about 100 ml of *P. antarctica* culture was gently (pressure < 0.5 mmHg) collected onto acid-cleaned 2-µm pore-size PC filters and rinsed three times for 2 min with 10 ml of Fe-free artificial seawater. Then, cells were resuspended in 7 to 8 ml of Fe-free artificial seawater (description below), resulting in an ~12 times concentrate culture from which 300 µl was taken and added to each subsample preequilibrated with ^{55}Fe. One milliliter from incubation bottles was systematically taken for immediate in vivo determination of Chl a fluorescence measurements (Turner Designs Inc.) and cell abundance to (i) verify similar addition of biomass between samples and (ii) further normalize Fe uptake rates among incubation bottles. Cell abundance was determined using a cell counter and analyzer system CASY Model TTC (Roche Innovartis, Reutlingen, Germany) equipped with a 60-µm capillary. The incubation began the moment cells were inoculated and lasted for 24 hours in the dark. All manipulations and incubations were conducted at 4°C. One subsample served as blank control by incubating killed cells (2% formaldehyde) and was treated identically.

After the 24-hour incubation time, cells were collected by filtration onto 2-µm pore-size nitrocellulose filters (Whatman). To remove any ^{55}Fe not internalized, cells were rinsed three times with 5 ml of titanium-citrate-EDTA solution (2-min contact time) followed by two rinses with 10 ml of 0.2-µm filtered seawater (1-min contact time) (*86*–*88*). Counts per minute (cpm) were determined using a Tri-Carb 2900TR liquid scintillation counter after 10-min analyses (PerkinElmer, MA, USA). Values from blanks accounted for nonbiologically mediated retention of ^{55}Fe on the filters (one blank per sample depth) and were subtracted from cpm measured for the corresponding depth. The results were transformed into disintegrations per minute at reference date considering the specific activity of ^{55}Fe source and the counting efficiency by the scintillation counter (calculated using the quenching factor determined for each sample and the regression equation of a homemade quenching curve using acetonitrile as quenching agent). Intracellular Fe uptake rates (ρFe_{int}, in mol Fe $hour^{-1}$ per cell) were obtained following normalization by filtered volume, incubation time, and cell abundance

$$\rho Fe_{int=}(Q \times {}^{55}Fe_{filter})/(\text{incubation time} \times \text{cell abundance})$$

with Q = (dFe in situ + ^{55}Fe added)/^{55}Fe added

and

$^{55}Fe_{filter}$ = (CPM sample − CPM blank)/(^{55}Fe specific activity × counting efficiency)

Calculation of Fe uptake rate constants—k_{int}

To evaluate the relative dFe bioavailability of SO seawater from our Fe uptake experiments, it was necessary to also determine Fe uptake rate constants by cells in seawater free of any ligands. Therefore, we performed additional incubations to calculate Fe internalization rate constants (k_{int}) by our model organism (*36*, *38*, *50*). To do so, *P. antarctica* was inoculated in incubation bottles with artificial seawater AQUIL medium [modified by the absence of the TM-buffered EDTA; (*89*)] containing different additions of inorganic ^{55}Fe ($^{55}FeCl_3$, as above). The k_{int} was determined from the slope of the linear increase of intracellular Fe uptake rate as a function of various dFe concentrations ranging between 0.3 and 0.7 nmol/liter and was 2.28×10^{-10} liter $cell^{-1}$ $hour^{-1}$. Despite Chelex treatment (Chelex 100 ion exchange resin, Bio-Rad), our synthetic medium contained

0.22 nmol/liter background dFe, which was considered in our calculation. When dFe is not complexed by ligands and is below the solubility limit of Fe(III), which is the case in our artificial seawater, total dFe therefore equals the dFe′ concentration in the medium.

The k_{int} was used to further estimate the relative bioavailability of Fe complexed to natural ligands (FeL). We compared the Fe uptake rates measured in natural seawater samples to those predicted from the k_{int} (by multiplying k_{int} with total dFe concentration of the sample). Given that Fe′ is considered as fully bioavailable (*15*, *20*, *36*) and that dFe is mainly bound to ligands in natural seawater (*90*), the comparison of Fe uptake in the presence (FeL) and in the absence (Fe′) of ligands provided a measure of the relative bioavailability of Fe across depths and stations. Therefore, here, we defined bioavailability (%) as the proportion of dFe uptake in the conditions tested (i.e., collected seawater with natural ligands) relative to the predicted Fe uptake rate using the k_{int} regression

$$\text{Bioavailability}\,(\%) = \rho\text{Fe}_{int}(\text{mol Fe cell}^{-1}\,\text{day}^{-1})/k_{int}(\text{liter cell}^{-1}\,\text{day}^{-1}) \times \text{dFe}\,(\text{mol Fe liter}^{-1}) \times 100$$

Fe uptake rates measured in our study were in good agreements with previous investigations on *P. antarctica*. For instance, (*49*) measured from 0.23 to 30.98 μmol Fe L_{CV}^{-1} $hour^{-1}$ (L_{CV}, cell volume in liter) in short term (8 to 15 hours) uptake of FeDFB (DFB) experiments by *P. antarctica* (clone AA1). Taking into account the difference in cell volume of our strain (14.5 fl $cell^{-1}$ versus 16.4 to 18.1 fl $cell^{-1}$ for clone AA1), we found similar values that ranged from 0.28 to 10.72 μmol Fe L_{CV}^{-1} $hour^{-1}$. Only station TMR12 is an exception (0.01 to 0.03 μmol Fe L_{CV}^{-1} $hour^{-1}$).

Calculating surface area–normalized Fe uptake rate constant —$k_{in\text{-}app}$/S.A.

To calculate the $k_{in\text{-}app}$, one assumption is that cells were accessing Fe mostly from the FeL pool. Fe uptake rates by *P. antarctica* greatly exceeded diffusive flux of equilibrium concentrations of Fe′ (table S1). This implies that cells mostly accessed Fe from the FeL pool, probably by the mean of extracellular reduction of the complexes. A second assumption made was that Fe uptake is linear (*37*) throughout the incubation experiment. For the uptake to remain linear, cells should not be affected by the depletion of the dFe (*37*), thereby the pool of dFe available should be substantially higher than Fe acquired by the cells. This criterion was also verified as we estimated that more than 95% of dFe at initial times were still available by the end of the incubation.

Statistics and data treatment

All data are given as the means and SDs of three biological replicates unless otherwise indicated. Correlation coefficients between Fe chemical speciation, Fe uptake rates, and estimated dFe bioavailability were determined using Pearson Product Moment. Data visualization and statistical analyses (correlations and PCA) were performed using SigmaPlot 11.0 (SysStat Software, CA, USA) and R Studio and package corrplot (*91*).

Supplementary Materials

This PDF file includes:

Figs. S1 to S4
Tables S1 and S2

View/request a protocol for this paper from *Bio-protocol*.

REFERENCES AND NOTES

1. J. H. Martin, Glacial-interglacial CO_2 change: The iron hypothesis. *Paleoceanography* **5**, 1–13 (1990).
2. C. Völker, A. Tagliabue, Modeling organic iron-binding ligands in a three-dimensional biogeochemical ocean model. *Mar. Chem.* **173**, 67–77 (2015).
3. Y. Shaked, B. S. Twining, A. Tagliabue, M. T. Maldonado, Probing the bioavailability of dissolved iron to marine eukaryotic phytoplankton using in situ single cell iron quotas. *Global Biogeochem. Cycles* **35**, e2021GB006979 (2021).
4. A. Tagliabue, L. Bopp, O. Aumont, K. R. Arrigo, Influence of light and temperature on the marine iron cycle: From theoretical to global modeling. *Global Biogeochem. Cycles* **23**, GB2017 (2009).
5. SCOR Working Group, GEOTRACES–An international study of the global marine biogeochemical cycles of trace elements and their isotopes. *Chemie der Erde* **67**, 85–131 (2007).
6. R. Schlitzer, R. F. Anderson, E. M. Dodas, M. Lohan, W. Geibert, A. Tagliabue, A. Bowie, C. Jeandel, M. T. Maldonado, W. M. Landing, D. Cockwell, C. Abadie, W. Abouchami, E. P. Achterberg, A. Agather, A. Aguliar-Islas, H. M. van Aken, M. Andersen, C. Archer, M. Auro, H. J. de Baar, O. Baars, A. R. Baker, K. Bakker, C. Basak, M. Baskaran, N. R. Bates, D. Bauch, P. van Beek, M. K. Behrens, E. Black, K. Bluhm, L. Bopp, H. Bouman, K. Bowman, J. Bown, P. Boyd, M. Boye, E. A. Boyle, P. Branellec, L. Bridgestock, G. Brissebrat, T. Browning, K. W. Bruland, H.-J. Brumsack, M. Brzezinski, C. S. Buck, K. N. Buck, K. Buesseler, A. Bull, E. Butler, P. Cai, P. C. Mor, D. Cardinal, C. Carlson, G. Carrasco, N. Casacuberta, K. L. Casciotti, M. Castrillejo, E. Chamizo, R. Chance, M. A. Charette, J. E. Chaves, H. Cheng, F. Chever, M. Christl, T. M. Church, I. Closset, A. Colman, T. M. Conway, D. Cossa, P. Croot, J. T. Cullen, G. A. Cutter, C. Daniels, F. Dehairs, F. Deng, H. T. Dieu, B. Duggan, G. Dulaquais, C. Dumousseaud, Y. Echegoyen-Sanz, R. L. Edwards, M. Ellwood, E. Fahrbach, J. N. Fitzsimmons, A. R. Flegal, M. Q. Fleisher, T. van de Flierdt, M. Frank, J. Friedrich, F. Fripiat, H. Fröllje, S. J. G. Galer, T. Gamo, R. S. Ganeshram, J. Garcia-Orellana, E. Garcia-Solsona, M. Gault-Ringold, E. George, L. J. A. Gerringa, M. Gilbert, J. M. Godoy, S. L. Goldstein, S. R. Gonzalez, K. Grissom, C. Hammerschmidt, A. Hartman, C. S. Hassler, E. C. Hathorne, M. Hatta, N. Hawco, C. T. Hayes, L.-E. Heimbürger, J. Helgoe, M. Heller, G. M. Henderson, P. B. Henderson, S. van Heuven, P. Ho, T. J. Horner, Y.-T. Hsieh, K.-F. Huang, M. P. Humphreys, K. Isshiki, J. E. Jacquot, D. J. Janssen, W. J. Jenkins, S. John, E. M. Jones, J. L. Jones, D. C. Kadko, R. Kayser, T. C. Kenna, R. Khondoker, T. Kim, L. Kipp, J. K. Klar, M. Klunder, S. Kretschmer, Y. Kumamoto, P. Laan, M. Labatut, F. Lacan, P. J. Lam, M. Lambelet, C. H. Lamborg, F. A. C. Le Moigne, E. Le Roy, O. J. Lechtenfeld, J.-M. Lee, P. Lherminier, S. Little, M. López-Lora, Y. Lu, P. Masque, E. Mawji, C. R. Mcclain, C. Measures, S. Mehic, J.-L. M. Barraqueta, P. van der Merwe, R. Middag, S. Mieruch, A. Milne, T. Minami, J. W. Moffett, G. Moncoiffe, W. S. Moore, P. J. Morris, P. L. Morton, Y. Nakaguchi, N. Nakayama, J. Niedermiller, J. Nishioka, A. Nishiuchi, A. Noble, H. Obata, S. Ober, D. C. Ohnemus, J. van Ooijen, J. O'Sullivan, S. Owens, K. Pahnke, M. Paul, F. Pavia, L. D. Pena, B. Peters, F. Planchon, H. Planquette, C. Pradoux, V. Puigcorbé, P. Quay, F. Queroue, A. Radic, S. Rauschenberg, M. Rehkämper, R. Rember, T. Remenyi, J. A. Resing, J. Rickli, S. Rigaud, M. J. A. Rijkenberg, S. Rintoul, L. F. Robinson, M. Roca-Martí, V. Rodellas, T. Roeske, J. M. Rolison, M. Rosenberg, S. Roshan, M. M. R. van der Loeff, E. Ryabenko, M. A. Saito, L. A. Salt, V. Sanial, G. Sarthou, C. Schallenberg, U. Schauer, H. Scher, C. Schlosser, B. Schnetger, P. Scott, P. N. Sedwick, I. Semiletov, R. Shelley, R. M. Sherrell, A. M. Shiller, D. M. Sigman, S. K. Singh, H. A. Slagter, E. Slater, W. M. Smethie, H. Snaith, Y. Sohrin, B. Sohst, J. E. Sonke, S. Speich, R. Steinfeldt, G. Stewart, T. Stichel, C. H. Stirling, J. Stutsman, G. J. Swarr, J. H. Swift, A. Thomas, K. Thorne, C. P. Till, R. Till, A. T. Townsend, E. Townsend, R. Tuerena, B. S. Twining, D. Vance, S. Velazquez, C. Venchiarutti, M. Villa-Alfageme, S. M. Vivancos, A. H. L. Voelker, B. Wake, M. J. Warner, R. Watson, E. van Weerlee, M. A. Weigand, Y. Weinstein, D. Weiss, A. Wisotzki, E. M. S. Woodward, J. Wu, Y. Wu, K. Wuttig, N. Wyatt, Y. Xiang, R. C. Xie, Z. Xue, H. Yoshikawa, J. Zhang, P. Zhang, Y. Zhao, L. Zheng, X.-Y. Zheng, M. Zieringer, L. A. Zimmer, P. Ziveri, P. Zunino, C. Zurbrick, The GEOTRACES intermediate data product 2017. *Chem. Geol.* **493**, 210–223 (2018).
7. J. K. Moore, K. Lindsay, S. C. Doney, M. C. Long, K. Misumi, Marine ecosystem dynamics and biogeochemical cycling in the community earth system model [CESM1(BGC)]: Comparison of the 1990s with the 2090s under the RCP4.5 and RCP8.5 scenarios. *J. Climate* **26**, 9291–9312 (2013).
8. A. Tagliabue, J. B. Sallée, A. R. Bowie, M. Lévy, S. Swart, P. W. Boyd, Surface-water iron supplies in the Southern Ocean sustained by deep winter mixing. *Nat. Geosci.* **7**, 314–320 (2014).
9. M. Sieber, T. M. Conway, G. F. de Souza, C. S. Hassler, M. J. Ellwood, D. Vance, Isotopic fingerprinting of biogeochemical processes and iron sources in the iron-limited surface Southern Ocean. *Earth Planet. Sci. Lett.* **567**, 116967 (2021).

10. R. F. Anderson, GEOTRACES: Accelerating research on the marine biogeochemical cycles of trace elements and their isotopes. *Ann. Rev. Mar. Sci.* **12**, 49–85 (2020).
11. T. M. Conway, T. J. Horner, Y. Plancherel, A. G. González, A decade of progress in understanding cycles of trace elements and their isotopes in the oceans. *Chem. Geol.* **580**, 120381 (2021).
12. R. M. Boiteau, D. R. Mende, N. J. Hawco, M. R. McIlvin, J. N. Fitzsimmons, M. A. Saito, P. N. Sedwick, E. F. DeLong, D. J. Repeta, Siderophore-based microbial adaptations to iron scarcity across the eastern Pacific Ocean. *Proc. Natl. Acad. Sci.* **113**, 14237–14242 (2016).
13. R. M. Boiteau, D. J. Repeta, Slow kinetics of iron binding to marine ligands in seawater measured by isotope exchange liquid chromatography–inductively coupled plasma mass spectrometry. *Environ. Sci. Technol.* **56**, 3770–3779 (2022).
14. H. M. Macrellis, C. G. Trick, E. L. Rue, G. J. Smith, K. W. Bruland, Collection and detection of natural iron-binding ligands from seawater. *Mar. Chem.* **76**, 175–187 (2001).
15. F. M. M. Morel, A. B. Kustka, Y. Shaked, The role of unchelated Fe in the iron nutrition of phytoplankton. *Limnol. Oceanogr.* **53**, 400–404 (2008).
16. C. Hassler, V. Schoemann, M. Boye, A. Tagliabue, M. Rozmarynowycz, R. M. L. Mckay, Iron bioavailability in the Southern Ocean, in *Oceanography and Marine Biology* (CRC Press, ed. 1, 2012), pp. 10–73; https://taylorfrancis.com/chapters/edit/10.1201/b12157-3/iron-bioavailability-southern-ocean-hassler-schoemann-boye-tagliabue-rozmarynowycz-mckay.
17. N. J. Hawco, F. Fu, N. Yang, D. A. Hutchins, S. G. John, Independent iron and light limitation in a low-light-adapted *Prochlorococcus* from the deep chlorophyll maximum. *ISME J.* **15**, 359–362 (2021).
18. M. Gledhill, K. N. Buck, The organic complexation of iron in the marine environment: A review. *Front. Microbiol.* **3**, 69 (2012).
19. L. M. Laglera, A. Tovar-Sanchez, C. F. Sukekava, H. Naik, S. W. A. Naqvi, D. A. Wolf-Gladrow, Iron organic speciation during the LOHAFEX experiment: Iron ligands release under biomass control by copepod grazing. *J. Mar. Syst.* **207**, 103151 (2020).
20. Y. Shaked, A. B. Kustka, F. M. M. Morel, A general kinetic model for iron acquisition by eukaryotic phytoplankton. *Limnol. Oceanogr.* **50**, 872–882 (2005).
21. D. J. E. Cabanes, L. Norman, A. R. Bowie, S. Strme˘ki, C. Hassler, Electrochemical evaluation of iron-binding ligands along the Australian GEOTRACES southwestern Pacific section (GP13). *Mar. Chem.* **219**, 103736 (2020).
22. C. Hassler, F. E. Legiret, E. C. V. Butler, Measurement of iron chemical speciation in seawater at 4°C: The use of competitive ligand exchange–adsorptive cathodic stripping voltammetry. *Mar. Chem.* **149**, 63–73 (2013).
23. R. M. Bundy, R. M. Boiteau, C. McLean, K. A. Turk-Kubo, M. R. McIvin, M. A. Saito, B. A. S. Van Mooy, D. J. Repeta, Distinct siderophores contribute to iron cycling in the mesopelagic at station ALOHA. *Front. Mar. Sci.* **5**, 1–15 (2018).
24. C. Hassler, D. Cabanes, S. Blanco-Ameijeiras, S. G. Sander, R. Benner, Importance of refractory ligands and their photodegradation for iron oceanic inventories and cycling. *Mar. Freshw. Res.* **71**, 311–320 (2019).
25. Y. Shaked, H. Lis, Disassembling iron availability to phytoplankton. *Front. Microbiol.* **3**, 123 (2012).
26. C. W. S. Chen, E. M. H. Lin, F.-C. Liu, R. H. Gerlach, Bayesian estimation for parsimonious threshold autoregressive models in {R}. *R News* **8**, 26–33 (2008).
27. D. A. Hutchins, A. E. Witter, A. Butler, G. L. Luther III, Competition among marine phytoplankton for different chelated iron species. *Nature* **400**, 858–861 (1999).
28. C. S. Hassler, C. M. G. van den Berg, P. W. Boyd, Toward a regional classification to provide a more inclusive examination of the ocean biogeochemistry of iron-binding ligands. *Front. Mar. Sci.* **4**, 10.3389/fmars.2017.00019, (2017).
29. H. Whitby, M. Bressac, G. Sarthou, M. J. Ellwood, C. Guieu, P. W. Boyd, Contribution of electroactive humic substances to the iron-binding ligands released during microbial remineralization of sinking particles. *Geophys. Res. Lett.* **47**, e2019GL086685 (2020).
30. L. M. Laglera, C. M. G. Van Den Berg, Evidence for geochemical control of iron by humic substances in seawater. *Limnol. Oceanogr.* **54**, 610–619 (2009).
31. C. Hassler, V. Schoemann, Bioavailability of organically bound Fe to model phytoplankton of the Southern Ocean. *Biogeosciences* **6**, 2281–2296 (2009).
32. B. S. Twining, S. B. Baines, The trace metal composition of marine phytoplankton. *Ann. Rev. Mar. Sci.* **5**, 191–215 (2013).
33. A. Marchetti, D. M. Schruth, C. A. Durkin, M. S. Parker, R. B. Kodner, C. T. Berthiaume, R. Morales, A. E. Allen, E. V. Armbrust, Comparative metatranscriptomics identifies molecular bases for the physiological responses of phytoplankton to varying iron availability. *Proc. Natl. Acad. Sci. U.S.A.* **109**, E317–E325 (2012).
34. R. F. Strzepek, P. W. Boyd, W. G. Sunda, Photosynthetic adaptation to low iron, light, and temperature in Southern Ocean phytoplankton. *Proc. Natl. Acad. Sci. U.S.A.* **116**, 4388–4393 (2019).
35. R. Sutak, J.-M. Camadro, E. Lesuisse, Iron uptake mechanisms in marine phytoplankton. *Front. Microbiol.* **11**, 566691 (2020).
36. H. Lis, Y. Shaked, C. Kranzler, N. Keren, F. M. M. Morel, Iron bioavailability to phytoplankton: An empirical approach. *ISME J.* **9**, 1003–1013 (2015).
37. Y. Shaked, K. N. Buck, T. Mellett, M. T. Maldonado, Insights into the bioavailability of oceanic dissolved Fe from phytoplankton uptake kinetics. *ISME J.* **14**, 1182–1193 (2020).
38. R. J. M. Hudson, F. M. M. Morel, Iron transport in marine phytoplankton: Kinetics of cellular and medium coordination reactions. *Limnol. Oceanogr.* **35**, 1002–1020 (1990).
39. W. G. Sunda, S. A. Huntsman, Iron uptake and growth limitation in oceanic and coastal phytoplankton. *Mar. Chem.* **50**, 189–206 (1995).
40. S. Blanco-Ameijeiras, D. J. E. Cabanes, R. N. Cable, S. Trimborn, S. Jacquet, S. Wiegmann, C. Völkner, F. Lelchat, A. Bracher, M. B. Duhaime, C. S. Hassler, Exopolymeric substances control microbial community structure and function by contributing to both c and fe nutrition in fe-limited southern ocean provinces. *Microorganisms* **8**, 1980 (2020).
41. D. J. E. Cabanes, S. Blanco-Ameijeiras, K. Bergin, S. Trimborn, C. Völkner, F. Lelchat, C. Hassler, Using Fe chemistry to predict Fe uptake rates for natural plankton assemblages from the Southern Ocean. *Mar. Chem.* **225**, 103853 (2020).
42. C. M. S. Schine, A.-C. Alderkamp, G. van Dijken, L. J. A. Gerringa, S. Sergi, P. Laan, H. van Haren, W. H. van de Poll, K. R. Arrigo, Massive Southern Ocean phytoplankton bloom fed by iron of possible hydrothermal origin. *Nat. Commun.* **12**, 1211 (2021).
43. P. N. Sedwick, N. S. Garcia, S. F. Riseman, C. M. Marsay, G. R. DiTullio, Evidence for high iron requirements of colonial Phaeocystis antarctica at low irradiance. *Biogeochemistry* **83**, 83–97 (2007).
44. V. Schoemann, S. Becquevort, J. Stefels, V. Rousseau, C. Lancelot, Phaeocystis blooms in the global ocean and their controlling mechanisms: A review. *J. Sea Res.* **53**, 43–66 (2005).
45. D. Antoine, S. Thomalla, D. Berliner, H. Little, W. Moutier, A. Olivier, C. Robinson, T. Ryan-Keogh, N. Schuback, Phytoplankton pigment concentrations of seawater sampled during the Antarctic Circumnavigation Expedition (ACE) during the Austral Summer of 2016/2017 (Version 1.1) (2020); https://doi.org/10.5281/zenodo.3816726.
46. D. J. Janssen, M. Sieber, M. J. Ellwood, T. M. Conway, P. M. Barrett, X. Chen, G. F. de Souza, C. S. Hassler, S. L. Jaccard, Trace metal and nutrient dynamics across broad biogeochemical gradients in the Indian and Pacific sectors of the Southern Ocean. *Mar. Chem.* **221**, 103773 (2020).
47. D. A. Siegel, T. DeVries, I. Cetinić, K. M. Bisson, Quantifying the ocean's biological pump and its carbon cycle impacts on global scales. *Ann. Rev. Mar. Sci.* **15**, 329–356 (2023).
48. D. Hansell, C. Carlson, D. Repeta, R. Schlitzer, Dissolved organic matter in the ocean: A controversy stimulates new insights. *Oceanography* **22**, 202–211 (2009).
49. R. F. Strzepek, M. T. Maldonado, K. A. Hunter, R. D. Frew, P. W. Boyd, Adaptive strategies by Southern Ocean phytoplankton to lessen iron limitation: Uptake of organically complexed iron and reduced cellular iron requirements. *Limnol. Oceanogr.* **56**, 1983–2002 (2011).
50. C. S. Hassler, V. Schoemann, C. M. Nichols, E. C. V. Butler, P. W. Boyd, Saccharides enhance iron bioavailability to Southern Ocean phytoplankton. *Proc. Natl. Acad. Sci. U.S.A.* **108**, 1076–1081 (2011).
51. F. Koch, S. Beszteri, L. Harms, S. Trimborn, The impacts of iron limitation and ocean acidification on the cellular stoichiometry, photophysiology, and transcriptome of *Phaeocystis antarctica*. *Limnol. Oceanogr.* **64**, 357–375 (2019).
52. J. B. McQuaid, A. B. Kustka, M. Oborník, A. Horák, J. P. McCrow, B. J. Karas, H. Zheng, T. Kindeberg, A. J. Andersson, K. A. Barbeau, A. E. Allen, Carbonate-sensitive phytotransferrin controls high-affinity iron uptake in diatoms. *Nature* **555**, 534–537 (2018).
53. X. Gao, C. Bowler, E. Kazamia, Iron metabolism strategies in diatoms. *J. Exp. Bot.* **72**, 2165–2180 (2021).
54. R. Raiswell, J. Hawkings, A. Elsenousy, R. Death, M. Tranter, J. Wadham, Iron in glacial systems: Speciation, reactivity, freezing behavior, and alteration during transport. *Front. Earth Sci.* **6**, 222 (2018).
55. R. Raiswell, L. G. Benning, M. Tranter, S. Tulaczyk, Bioavailable iron in the Southern Ocean: The significance of the iceberg conveyor belt. *Geochem. Trans.* **9**, 7 (2008).
56. K. R. Arrigo, Phytoplankton dynamics within 37 Antarctic coastal polynya systems. *J. Geophys. Res.* **108**, 3271 (2003).
57. M. Sieber, T. M. Conway, G. F. de Souza, C. Hassler, M. J. Ellwood, D. Vance, Cycling of zinc and its isotopes across multiple zones of the Southern Ocean: Insights from the Antarctic circumnavigation expedition. *Geochim. Cosmochim. Acta* **268**, 310–324 (2020).
58. C. Lory, F. Van Wambeke, M. Fourquez, A. Barani, C. Guieu, C. Tilliette, D. Marie, S. Nunige, I. Berman-Frank, S. Bonnet, Assessing the contribution of diazotrophs to microbial Fe uptake using a group specific approach in the western tropical South Pacific Ocean. *ISME Commun.* **2**, 41 (2022).
59. H. E. Garcia, R. A. Locarnini, T. P. Boyer, J. I. Antonov, O. K. Baranova, M. M. Zweng, J. R. Reagan, D. R. Johnson, in *World Ocean Atlas 2013, Volume 4 : Dissolved Inorganic Nutrients (phosphate, nitrate, silicate)* (NOAA Atlas NESDIS 76, 2013), vol. 4.
60. M. T. Maldonado, R. F. Strzepek, S. Sander, P. W. Boyd, Acquisition of iron bound to strong organic complexes, with different Fe binding groups and photochemical reactivities, by

plankton communities in Fe-limited subantarctic waters. *Glob. Biogeochem. Cycles* 19, 10. 1029/2005GB002481, (2005).
61. M. T. Maldonado, N. M. Price, Utilization of iron bound to strong organic ligands by plankton communities in the subarctic Pacific Ocean. *Deep Sea Res. II: Top. Stud. Oceanogr.* **46**, 2447–2473 (1999).
62. A. L. King, K. N. Buck, K. A. Barbeau, Quasi-Lagrangian drifter studies of iron speciation and cycling off Point Conception, California. *Mar. Chem.* **128**, 1–12 (2012).
63. M. Fourquez, R. F. Strzepek, M. J. Ellwood, C. Hassler, D. Cabanes, S. Eggins, I. Pearce, S. Deppeler, T. W. Trull, P. W. Boyd, M. Bressac, Phytoplankton responses to bacterially regenerated iron in a Southern Ocean eddy. *Microorganisms* **10**, 1655 (2022).
64. D. L. Kirchman, Microbial ferrous wheel. *Nature* **383**, 303–304 (1996).
65. A. Tagliabue, C. Völker, Towards accounting for dissolved iron speciation in global ocean models. *Biogeosciences* **8**, 3025–3039 (2011).
66. D. König, T. M. Conway, M. J. Ellwood, W. B. Homoky, A. Tagliabue, Constraints on the cycling of iron isotopes from a global ocean model. *Global Biogeochem. Cycles* **35**, e2021GB006968 (2021).
67. J. N. Fitzsimmons, T. M. Conway, Novel insights into marine iron biogeochemistry from iron isotopes. *Ann. Rev. Mar. Sci.* **15**, 383–406 (2023).
68. M. J. Ellwood, D. A. Hutchins, M. C. Lohan, A. Milne, P. Nasemann, S. D. Nodder, S. G. Sander, R. Strzepek, S. W. Wilhelm, P. W. Boyd, Iron stable isotopes track pelagic iron cycling during a subtropical phytoplankton bloom. *Proc. Natl. Acad. Sci. U.S.A.* **112**, E15–E20 (2015).
69. D. S. Mulholland, F. Poitrasson, L. S. Shirokova, A. G. González, O. S. Pokrovsky, G. R. Boaventura, L. C. Vieira, Iron isotope fractionation during Fe(II) and Fe(III) adsorption on cyanobacteria. *Chem. Geol.* **400**, 24–33 (2015).
70. M. J. Ellwood, R. F. Strzepek, P. G. Strutton, T. W. Trull, M. Fourquez, P. W. Boyd, Distinct iron cycling in a Southern Ocean eddy. *Nat. Commun.* **11**, 825 (2020).
71. S. L. Brantley, L. J. Liermann, R. L. Guynn, A. Anbar, G. A. Icopini, J. Barling, Fe isotopic fractionation during mineral dissolution with and without bacteria. *Geochim. Cosmochim. Acta* **68**, 3189–3204 (2004).
72. S. M. Ilina, F. Poitrasson, S. A. Lapitskiy, Y. V. Alekhin, J. Viers, O. S. Pokrovsky, Extreme iron isotope fractionation between colloids and particles of boreal and temperate organic-rich waters. *Geochim. Cosmochim. Acta* **101**, 96–111 (2013).
73. K. Dideriksen, J. A. Baker, S. L. S. Stipp, Equilibrium Fe isotope fractionation between inorganic aqueous Fe(III) and the siderophore complex, Fe(III)-desferrioxamine B. *Earth Planet. Sci. Lett.* **269**, 280–290 (2008).
74. J. L. L. Morgan, L. E. Wasylenki, J. Nuester, A. D. Anbar, Fe isotope fractionation during equilibration of Fe−organic complexes. *Environ. Sci. Technol.* **44**, 6095–6101 (2010).
75. S. Landwehr, M. Volpi, F. A. Haumann, C. M. Robinson, I. Thurnherr, V. Ferracci, A. Baccarini, J. Thomas, I. Gorodetskaya, C. Tatzelt, S. Henning, R. L. Modini, H. J. Forrer, Y. Lin, N. Cassar, R. Simó, C. Hassler, A. Moallemi, S. E. Fawcett, N. Harris, R. Airs, M. H. Derkani, A. Alberello, A. Toffoli, G. Chen, P. Rodríguez-Ros, M. Zamanillo, P. Cortés-Greus, L. Xue, C. G. Bolas, K. C. Leonard, F. Perez-Cruz, D. Walton, J. Schmale, Exploring the coupled ocean and atmosphere system with a data science approach applied to observations from the Antarctic circumnavigation expedition. *Earth Syst. Dynam.* **12**, 1295–1369 (2021).
76. W. Abouchami, S. J. G. Galer, H. J. W. de Baar, A. C. Alderkamp, R. Middag, P. Laan, H. Feldmann, M. O. Andreae, Modulation of the Southern Ocean cadmium isotope signature by ocean circulation and primary productivity. *Earth Planet. Sci. Lett.* **305**, 83–91 (2011).
77. A. Tagliabue, A. R. Bowie, P. W. Boyd, K. N. Buck, K. S. Johnson, M. A. Saito, The integral role of iron in ocean biogeochemistry. *Nature* **543**, 51–59 (2017).
78. G. Cutter, K. Casciotti, P. Croot, W. Geibert, L.-E. Heimbürger, M. Lohan, H. Planquette, T. van de Flierdt, in *Sampling and Sample-handling Protocols for GEOTRACES Cruises* (GEOTRACES International Project Office Toulouse, France, 2017); https://geotraces.org/methods-cookbook/.
79. S. M. Myklestad, E. Skanoy, S. Hestmann, A sensitive and rapid method for analysis of dissolved mono- and polysaccharides in seawater. *Mar. Chem.* **56**, 279–286 (1997).
80. C. Hassler, Hydrolysable carbohydrate data collected from the Trace Metal Rosette in the Southern Ocean during the austral summer of 2016/2017, on board the Antarctic Circumnavigation Expedition (2019); doi.org/10.5281/zenodo.2635686.
81. M. Sieber, T. M. Conway, G. F. de Souza, C. S. Hassler, M. J. Ellwood, D. Vance, High-resolution Cd isotope systematics in multiple zones of the Southern Ocean from the Antarctic circumnavigation expedition. *Earth Planet. Sci. Lett.* **527**, 115799 (2019).
82. S. J. Bender, D. M. Moran, M. R. McIlvin, H. Zheng, J. P. McCrow, J. Badger, G. R. DiTullio, A. E. Allen, M. A. Saito, Colony formation in *Phaeocystis antarctica*: Connecting molecular mechanisms with iron biogeochemistry. *Biogeosciences* **15**, 4923–4942 (2018).
83. S. Trimborn, S. Thoms, K. Bischof, S. Beszteri, Susceptibility of two Southern Ocean phytoplankton key species to iron limitation and high light. *Front. Mar. Sci.* **6**, 167 (2019).
84. D. J. Suggett, C. M. Moore, A. E. Hickman, R. J. Geider, Interpretation of fast repetition rate (FRR) fluorescence: Signatures of phytoplankton community structure versus physiological state. *Mar. Ecol. Prog. Ser.* **376**, 1–19 (2009).
85. X. Liu, F. J. Millero, The solubility of iron in seawater. *Mar. Chem.* **77**, 43–54 (2002).
86. D. Tang, F. M. M. Morel, Distinguishing between cellular and Fe-oxide-associated trace elements in phytoplankton. *Mar. Chem.* **98**, 18–30 (2006).
87. C. Hassler, V. Schoemann, Discriminating between intra- and extracellular metals using chemical extractions: An update on the case of iron. *Limnol. Oceanogr. Methods.* **7**, 479–489 (2009).
88. M. Fourquez, I. Obernosterer, S. Blain, A method for the use of the radiotracer ^{55}Fe for microautoradiography and CARD-FISH of natural bacterial communities. *FEMS Microbiol. Lett.* **337**, 132–139 (2012).
89. N. M. Price, G. I. Harrison, J. G. Hering, R. J. Hudson, P. M. V. Nirel, B. Palenik, F. M. M. Morel, Preparation and chemistry of the artificial algal culture medium Aquil. *Biol. Oceanogr.* **6**, 443–461 (1989).
90. E. L. Rue, K. W. Bruland, Complexation of iron(III) by natural organic ligands in the Central North Pacific as determined by a new competitive ligand equilibration/adsorptive cathodic stripping voltammetric method. *Mar. Chem.* **50**, 117–138 (1995).
91. R Core Team, R: A Language and Environment for Statistical Computing (2022); https://r-project.org/.

Acknowledgments: We are grateful to all scientists and support staff involved in the collection and analysis of samples, both at sea and on shore, especially C. Völker and T. Brenneis (AWI, Germany) for eHS measurements as well as K. Bergin for TPZT measurements. We also thank S. Fawcett (University of Cape Town, South Africa) and R. Simó (Institut de Ciències del Mar, Spain) who shared data on in situ biomass cell abundance and N. Cassar (Duke University, USA) and S. Bonnet (MIO, France) who provided valuable advices in the writing of this manuscript. We also thank M.-N. Houssais (LOCEAN, France) for the time devoted to the deployment and analysis of the CTD profiles. **Funding:** This study was supported by Project 16 of the Antarctic Circumnavigation Expedition (ACE). ACE was a scientific expedition that carried out under the auspices of the Swiss Polar Institute (SPI), supported by funding from the ACE Foundation and Ferring Pharmaceuticals. M.F. and C.H. were supported by the Swiss National Science Foundation (PP00P2_138955 and PP00P2_166197), and M.F. was further funded by the European Union's Horizon 2020 research and innovation program under the Marie Sklodowska-Curie grant agreement no. 894264 (BULLE-project) and by Grant ERC no. 101044637 (HOPE-project). In addition, publications fees for this article were covered by the Mediterranean Institute of Oceanography. **Author contributions:** Conceptualization: M.F. and C.H. Analysis: M.F., D.C., D.J.J., and M.S. Investigation: M.F., C.H., D.J.J., and T.M.C. Visualization: M.F. Supervision: C.H. Writing—original draft: M.F. Writing—review and editing: M.F., D.J.J., T.M.C., M.J.E., M.S., S.T., and C.H. **Competing interests:** The authors declare that they have no competing interests. **Data and materials availability:** All data needed to evaluate the conclusions in the paper are present in the paper and/or the Supplementary Materials.

Submitted 9 December 2022
Accepted 24 May 2023
Published 28 June 2023
10.1126/sciadv.adf9696